coatings

MDPI

*Communication*

# Light Scattering through a Drying Coating

**Riccardo Antonelli and Thomas E. Kodger ***

Physical Chemistry and Soft Matter, Wageningen University & Research, 6700 HK Wageningen, The Netherlands; riccardo.antonelli@wur.nl

* Correspondence: thomas.kodger@wur.nl

**Abstract:** Drying coatings undergo internal dynamic densification and rearrangement, which are challenging to discern with optical techniques due to their multiple scatterings of light. Experiments such as diffusing wave spectroscopy (DWS) and laser speckle imaging (LSI) leverage these multiple scatterings to reveal the in situ dynamics of the coating. In such experiments, the knowledge of the sample volume that can be accessed and therefore studied is fundamental, especially in cases of micrometer-scale coating thicknesses. In this paper, we present a robust and reliable method using transmission geometry to calculate the parameter $l^*$, defined as the transport light mean-free path, which is strongly related to the volume of the sample that light explores in DWS and LSI experiments. We show how this dynamic parameter can be measured for liquid and solid film samples and, crucially, in the case of time-evolving samples, such as drying coatings of paint or ink, which has not been previously explored. We present a series of model ink samples and discuss the evolution of their densification during drying through quantification of dynamic $l^*$.

**Keywords:** dynamic coating; drying ink; multiple light scattering; experimental technique

check for updates

**Citation:** Antonelli, R.; Kodger, T.E. Light Scattering through a Drying Coating. *Coatings* **2023**, *13*, 1873. https://doi.org/10.3390/coatings13111873

Academic Editor: Fulvia Villani

Received: 27 August 2023
Revised: 24 October 2023
Accepted: 26 October 2023
Published: 31 October 2023

**Copyright:** © 2023 by the authors. Licensee MDPI, Basel, Switzerland. This article is an open access article distributed under the terms and conditions of the Creative Commons Attribution (CC BY) license (https://creativecommons.org/licenses/by/4.0/).

## 1. Introduction

The purpose of a coating is to create a long-lasting physical layer on top of a target substrate through a dynamic solidification process, often via the drying or curing of an applied liquid dispersion of particles or pigments. Coatings can be applied to a surface using a number of methods, including inkjet printing, which is probably one of the most widespread technological applications of microfluidics [1–3]. Inkjet printing is a reliable method used to produce picoliter droplets, jetted at the desired spatial location to ensure the high resolution and fidelity of the output. The reduced liquid volume used in inkjet printing allows for faster drying of the coating, increasing the resolution of the output, while hindering the study of their dynamics due to the small dimensions of the droplets. Similarly, continuous coatings are often formulated to increase the drying rate without inducing physical instabilities such as cracking, cissing, or peeling, resulting in the fast evolving internal dynamics of the film [4–7]. Additionally, the substrates onto which these inks and coatings are often printed offer a large deal of complexity, especially in the case of porous substrates, such as paper or fabric, into which the fluid can be imbibed, altering the solidification process [8–10]. Due to the complexity of these processes, involving concomitant drying and imbibement, a general framework of a liquid interacting with a porous or nonporous material remains unclear, requiring research into experimental techniques that elucidate this highly dynamic process.

Techniques that utilize light scattering are ideal candidates for illuminating these internal dynamics as they noninvasively probe the internal dynamics of an evolving coating under industrial conditions. When light impinges onto an opaque material, such as a wet pigmented coating or ink, a fraction of the incoming photons are reflected off the interface, while others penetrate the sample, scattering off of the coating components before being diffusively backscattered or transmitted. Understanding which volume of the material is sampled by penetrating and diffusing photons is essential knowledge in

multiple light-scattering experiments including in diffusing wave spectroscopy (DWS) and laser speckle imaging (LSI). Extending the concept of DWS to an imaging format, LSI is a noninvasive technique that was originally developed as a medical imaging technique to measure under-skin or cerebral blood flow [11–13].

As this technique is extremely versatile, recently, it has been implemented in a number of applications in materials science [14], including for studying the drying of droplets and thin film [4,15], mechanical processes in art restoration [16], crack and fracture formation [17], and structural rearrangements in granular materials [18]. With LSI, a digital camera is used to acquire a large spatial region of the sample, which is illuminated with a homogeneous field of expanded coherent laser light. The main advantage of LSI over DWS is that each pixel on the sensor is representative of a portion of the sample, which can be expressed in $x, y$ coordinates, thus providing the spatial resolution that DWS lacks. The volume explored by the photons during an LSI experiment is dictated by the transport mean-free path $l^*$, which is often overlooked and not quantified, especially dynamically, i.e., $l^*(t)$. DWS and LSI experiments are performed at the limit where there is multiple scattering but not yet strong localization [19]; at this limit, photon paths inside a sample can be described within the diffusion approximation [20,21]. Importantly, this means that a photon must scatter a sufficient number of times for its path to approach the statistical limit of a random walk, i.e., the diffusive limit [22–24]. Only if photons exiting the material have scattered enough times to be well within the multiple scattering diffusive regime is the collected interference, or speckle pattern, a valid representation of the diffusing behavior of the photons interacting with the sample. The change in the speckle pattern represents the motion of the scatterers. Thus, the results obtained from DWS or LSI experiments are challenging to interpret without knowledge of the scattering volume explored in these light experiments.

Crucially, $l^*$ is a scalar quantity that expresses the extent of the multiple scatterings in a material [22,25,26]. It expresses the distance photons travel before their original orientation is entirely randomized, which, depending on the material, can range from several millimeters for only mildly opaque materials to single microns for highly scattering matrices [27]. The transport mean-free path depends on the size, concentration, and spatial organization of the scatterers, and the refractive index contrast between scatterers and their surrounding medium. Crucially, these factors dynamically change during the drying of a coating. The polarization effects of the scatters can also affect $l^*$ if their optical properties are not isotropic, such as when the scatterers are formed from crystalline polymers. Since $l^*$ is affected by a large number of static and dynamic factors, it cannot be accurately calculated a priori for composite materials, such as a coating; yet, knowledge of its magnitude is crucial for the quantitative interpretation of multiple scattering experiments. Moreover, approximations underlying the theory used to interpret LSI data require that the sample is at least thicker than several times $l^*$ [24], so precise knowledge of its value is crucial for cases where sample dimensions may become comparable to $l^*$, as is the case for small picoliter inkjet-printed droplets or thin coatings. Multiple experimental methods have been developed to determine $l^*$ for opaque materials, including enhanced coherent back-scattering [28,29], oblique angle illumination [30,31], photon time-of-travel distribution [32], laser wavelength modulation [33], speckle frequency domain correlation [34,35], and comparison of transmitted light intensity with a reference material of known $l^*$ [22,36].

In this paper, we highlight the challenges encountered when measuring this crucial material property and describe a facile instrument that robustly and reliably determines the dynamic magnitude of $l^*(t)$. We describe approach that determines $l^*$ using an optical transmission geometry using a reference sample of known transport mean-free path. Crucially, this method also allows for the calculation of $l^*(t)$ in a sample whose optical properties change over time. As $l^*$ decreases over time, the scattering volume explored by the scattered photons changes also decreases; thus, the interpretation of the resulting sample mobility also changes. This key conceptual approach has been previously unexplored in the study of drying paints and inks.

## 2. Materials and Methods

In multiple scattering transmission geometry or forward scattering experiments, where the incident laser light fully traverses the thickness of the sample, the intensity of light is measured using a detector placed on the opposing side of a sample from the laser source. See Figure 1 for the setup and the relative schematic for transmission geometry experiments [37–39]. Without a sample, the coherent and collimated beam is aligned to pass through a pinhole positioned in front of a PMT; a single-mode fiber optic, with a diameter of 4.5 µm, acts as a pinhole in this instrument. When a sample is inserted, light impinges upon a nontransparent sample of thickness $L$ with a light mean-free path $l^*$; only some of the photons scatter and emerge on the other side of the sample. After passing through the "analyzer" and pinhole, scattered photons finally reach the detector. Importantly, for experiments relying on multiple scattering, introducing an optical analyzer component in a crossed polarization scheme, compared to the source laser, in front of the detector, is convenient as only those photons whose original polarization has been sufficiently randomized due to numerous scattering events can pass the analyzer [40]. Singly scattered or transmitted photons, which have not lost their original polarization sufficiently, are blocked by the analyzer. If the photon light paths exiting the material are longer then several $l^*$ lengths, then the polarization state is completely randomized, while a photon that has not scattered conserves its original polarization. The role of the analyzer positioned before the pinhole serves to block the photons that conserve the original polarization and therefore have not scattered enough to be considered in the multiple scattering regime.

For samples of thickness $L$ and mean-free path $l^*$, when $L/l^* > 5$, the photons are considered to be in the multiple scattering regime and can be approximated as random walkers [25]. Thus, the number of photons that arrive at the detector, measured as normalized intensity, is correlated to $l^*$. It has been demonstrated that the transmitted intensity and $l^*$ parameter, when light absorption is negligible, are related through the following equation [22,41–43]:

$$T = \frac{I}{I_0} = \frac{5l^*}{3L}\left(1 + \frac{4l^*}{3L}\right)^{(-1)}. \quad (1)$$

Therefore, by using identical optical and geometrical components for different samples, an unknown $l^*$ value may be calculated through the absolute transmission light intensity $L$, and $l^*$ is known for different samples possessing a known $l^*$. Thus, with this approach, the transmission intensity values we record for a reference sample, which, in our case, is polystyrene particles dispersed in water of $l^*$ = 130 µm, are related directly to the transmission intensity value for a sample of unknown $l^*$. We calculate this parameter through Equation (1): the ratio of the two transmission values is equal to the ratio of the right-hand side of Equation (1) for the two samples. In this evaluation, we do not consider the absorption of the source laser light from a pigmented coating, such as the yellow ink used in this study, which would change the calculated $l^*$; a laser wavelength must always be chosen to minimize the absorption for a given series of samples. In this series of experiments, we used green laser light at 532 nm on yellow ink, which minimized absorption as the photon energy was above the band gap of the yellow pigment. However, some absorption was still present. This could be quantified using reflection spectroscopic measurement. We present these data in Appendix A, Figure A4. The reflected light intensity was measured on a 0.15 mm thick draw-down of yellow ink as the difference in the reflected intensity from a white reference card stock. These results show some absorption of the incident laser light but clearly off the absorption maxima for this yellow ink. Unfortunately, the complex interplay between the absorption and multiple scattering events on the transport of a photon through a nonwhite ink has received limited attention in the literature despite its clear importance [44].

*Instrument*

To measure the transmission intensities in a forward scattering geometry, we built a simple optical instrument, as presented in Figure 1. For this experiment, a laser source at 532 nm (cobalt) of 5 mW to 350 mW intensity was used with the absolute intensity controlled using software. The light was directed through a polarized filter (Thorlabs LPVISC050, Bergkirchen, Germany) which ensured only one particular state of polarization for the incident light. After a series of steering mirrors, the light impinged normal to the sample. On the opposite side of the sample, an analyzer was set in a cross-polarization scheme to the polarizer, which blocked unscattered photons and all photons with insufficiently short scattering paths, followed by a single mode fiber optic acting as a pinhole, and finally a dector, photomultiplier tube. This PMT was connected via RF cables to a digital autocorrelator (ALV-7002/USB, ALV Instrument, Langen, Germany), which, through dedicated software, produced both an autocorrelation $g_2$ function and the time averaged transmission intensity value.

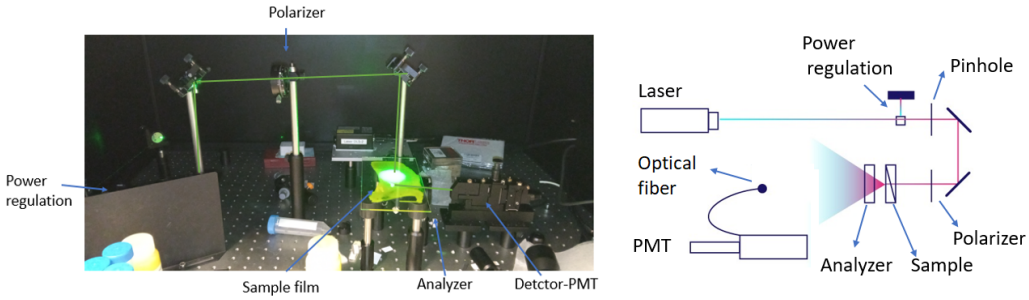


**Figure 1.** Instrumental setup for $l^*$ determination; a schematic is shown on the right.

Liquid samples were measured through a quartz cuvette 2.00 mm thick. Solid samples were placed on the optical path of the light, in the same position as the liquid filled cuvette. To measure the $l^*$ of solid heterogeneous samples, such as paper, the solid sample wasl slowly rotated off axis with the transmitted intensity recorded arising from different points of the sample and then averaged [45]. This ensures the photons experience multiple average paths, creating an averaged transmission light intensity signal avoiding discrete peaks or valleys.

For dynamic $l^*(t)$ experiments, ink films were prepared on a glass slide, with dimensions $5 \times 20 \times 0.15$ mm, with 0.15 mm being the initial optical path thickness. Data acquisition began seconds before the formation of the film over the glass. At this moment, the analyzer, which was set in cross-polarization mode to the incoming beam, served to fully block the beam at this position and avoid over-saturation of the detector. Using a doctor blade, containing a liquid reservoir, we scraped a film of 0.15 mm thickness over the glass slide. We recorded the first data point of the dynamic $l^*$ immediately after the film formed, with a time resolution of microseconds, defined by the PMT detector. Photons of the beam impinged the sample and multiply scattered inside the material, losing the initial phase, polarization, and propagation direction. Given the sample thickness $L$ was greater than $l^*$ by at least one order of magnitude, photons emerging on the detector side interfered each other, generating random constructive or destructive interference phases and polarization, and were therefore not blocked from the analyzer. A schematic of the possible photon paths is presented in Figure 2.

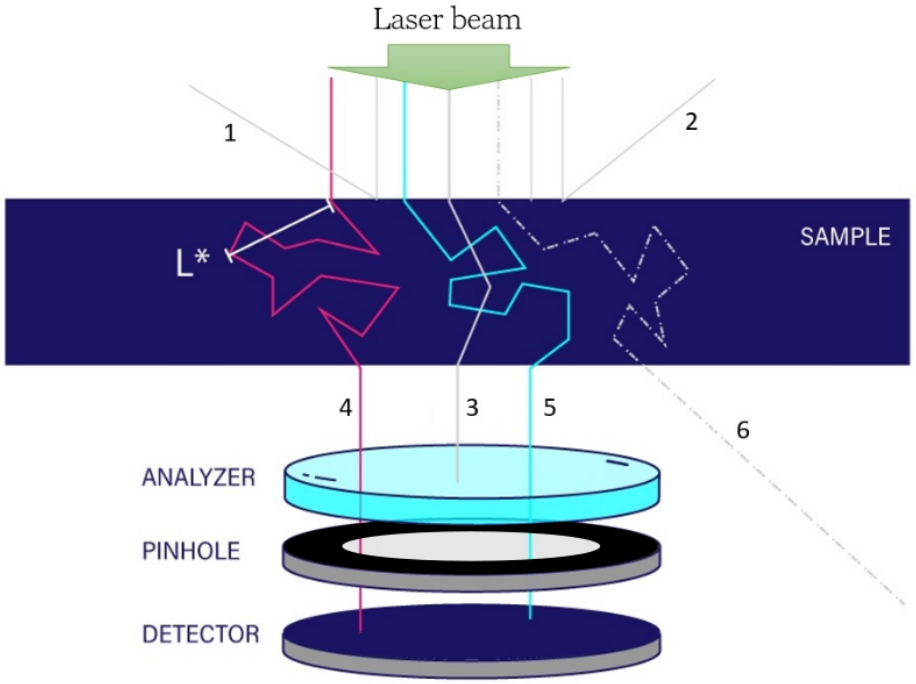


**Figure 2.** Schematic of the experimental setup in transmission geometry. An incoming laser beam impinges upon the sample from above in the vertical, normal direction to the sample surface. Some of the photons (1,2) are reflected from the surface without exploring the sample. Photons that have not scattered a sufficient number of times (3) conserve their original polarization and are blocked by the analyzer component. Photons that have scattered a sufficient number of times (4,5) and have travelled at least $\mathcal{O}(3l^*)$ lose their original polarization and are not blocked from the analyzer. After passing through a pinhole, a single-mode optical fiber, they reach the detector. Finally, many more photons (6) are scattered away, do not pass through the pinhole, and do not reach the detector.

The experiments performed in this transmission geometry were far more robust and easy to approach with respect to the calculation of $l^*$ than in he evaluation of the backscattered cone; this approach requires delicate alignment of the incident laser normal to sample container, high-precision and repeatable detection angles, and micrometer positional precision between the center of rotation and sample location. By contrast, in the transmission geometry, once the optical components are set in position and aligned, $l^*$ is repeatably evaluated for a number of samples, including solid, liquid, and drying coatings.

## 3. Results and Discussion

This instrument allows for the measurement of $l^*$ for a number of samples under multiple experimental conditions. This includes determining $l^*$ for nonevolving and evolving samples with time and nonevolving samples that do not change their internal structure during the timescale of the measurement, for example, a dispersion in a sealed cuvette. A schematic of the different processes arising during film formation is shown in Figure 3. An evolving sample is one where dynamic movement of internal structural occurs during the measurement, such as coalescence, or a phase change results in material refractive index modification, for example, scatterers that concentrate as the dispersed liquid phase evaporates as in the particular case of inks. Even prior to particle coalescence, deformations may modify the light paths inside the dispersion. These concomitant processes, which, in the case of picoliter ink droplets, happen at the timescale of one second, have a direct effect on the scattering properties of the material and therefore also on $l^*$, usually decreasing with time as the scatterer volume fraction increases.

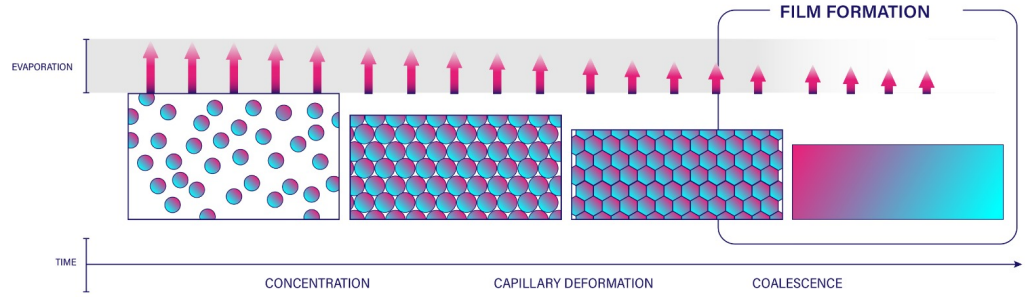


**Figure 3.** Schematic of drying processes and film formation for ink. In the first phase, particles, which, in our case, are latex particles, are dispersing and diffusing in a mixture of water and glycerol. After some time, the volatile phase evaporates, increasing the volume fraction of the scattering latex particles. The rate of evaporation decreases with time as the volume fraction increases. At a high volume fraction such that the particles nearly touch, internal capillary forces and deformation predominate and can cause particle deformation. Depending on the particular latex particles, coalescence and film formation can then occur if the latex has a sufficiently low glass transition temperature.

Not quantifying the magnitude of the change in $l^*$ may lead to the incorrect interpretation of the experiments that utilize multiple scattering. In the case of LSI measurement on inkjet-printed droplets, if $l^*$ increases above the physical dimension of the droplet, then the information recorded on scatterer mobility would not derive from the droplet volume itself, but rather be highly influenced by the motion of the underlying substrate.

### *3.1. Measuring $l^*$or Nonevolving Samples*

The starting point for all $l^*$ measurements is the calibration of the instrument through a measure of light transmission across the reference sample, i.e., a dispersion of polystyrene nanoparticles of a known volume fraction. Once this transmission value is established, the transmission light intensity is measured for an unknown sample with unknown $l^*$ but known $L$, the path length. Crucially, the same optical components and laser intensity must be used, only then can $l^*$ be calculated by means of Equation (1). A temporally stable laser source is crucial to measurement accuracy.

The measurement of $l^*$ for the model ink samples, detailed in the Materials section, is shown in Table 1. The upper panel shows the value of $l^*$ for liquid samples, with the lower panel showing $l^*$ for solid-phase samples. The variation in $l^*$ between these yellow pigmented inks is small, varying by less than a factor of two. These samples, as for the reference liquid, were measured in a sealed cuvette of precise thickness, $L = 2.00$ mm. However, while the solid-phase paper substrates resulted in $l^*$ values on same order of magnitude as the fluid samples, the solid plastic substrate, mylar, and a polymeric elastomer, PDMS with embedded 1 wt% titanium nanoparticles, showed higher values of $l^*$.

**Table 1.** Calculated $l^*$ values for nondrying samples. Liquid samples in the upper section and solid samples in the lower. More information concerning the ink composition is given in the Appendix A.

| Sample | Measured $l^*(t = 0)$ (μm) |
|---|---|
| ink A | $5.1 \pm 0.9$ |
| ink B | $5.1 \pm 1.1$ |
| ink C | $8.3 \pm 1.5$ |
| ink D | $3.3 \pm 0.5$ |
| commercial paper | $4.2 \pm 0.2$ |
| teslin paper | $4.9 \pm 0.2$ |
| mylar | $9.7 \pm 0.5$ |
| elastomer | $150 \pm 5$ |

These results demonstrate that DWS or LSI measurements obtained on ink picoliter or very thin coatings yield valid and reliable outcomes. The collected photons can be treated as having taken a random walk within the sample, as the magnitude of $l^*$ is similar to the sample's physical dimensions. Photons travel at least a few $l^*$ lengths inside a droplet volume. The role of the analyzer here is important, as it blocks reflected photons and photons that have not been scattered sufficiently to be randomly polarized; therefore, they have traveled path lengths shorter than $l^*$. Since $l^*$, a thin coating, and a picoliter droplet size are similar, there is a high probability that some if not most of the impinging light explores only a fraction of the scattering sample volume and therefore is blocked by the analyzer. Without this optical element, the measured intensity values needed for Equation (1) are found to be inconsistent and sensitive to sample positioning.

### *3.2. Measuring l*or Drying Liquid Films*

When a liquid dispersion film or droplet dries, concomitant physical processes affect the scattering properties of the material, i.e., $l^*$, to an unknown magnitude. Only when $l^*(t)$ remains smaller than the physical size of the coating or droplet can we consider the light as performing random walk thorough the sample, and we can apply the diffusion approximation, leading to accurate interpretation for the $g_1(t, \tau)$ autocorrelation functions in DWS or LSI experiments. Given the difficulty of measuring changes in $l^*$ for individual inkjet-printed micrometer/picoliter droplets, here, $l^*$ is measured for an ink film of a known thickness of $L$ = 0.150 mm, with this initial height of the sample being achieved through the use of a doctor blade. In a separate measurement, the weight of the sample is recorded with time for each of the four inks at the same ambient conditions as the $l^*(t)$ measurements. Recorded data are normalized and fit using a Gaussian biexponential model, which best describes the mass decay. Assuming the same decay for the sample height, $L(t)$ is computed as the film dries. Crucially, this change in thickness is taken into account when calculating $l^*(t)$ through Equation (1). The mass loss is shown in the inset in Figure 4: the normalized mass (%) as a function of time for the first 5000 s after film preparation appears to follow a *quasi*-linear drying rate, which reduces over time. The full picture of the mass loss for the four inks at longer times is reported in Appendix A, Figure A1, where after approximately $10^4$ s, the normalized mass stabilizes to approximately 40% of the initial value for all the ink dispersions under investigation. Once $L(t)$ is known, $l^*(t)$ can be calculated from the dynamic transmitted light intensity with a time resolution of a millisecond, as shown in Figure 4 for four model inks averaged over repeats.

While each film does show a decrease in $l^*(t)$, ink A follows a more complex change. Around a film drying time of 500 s, a relative rapid increase in $l^*$ is followed by rapid decrease in $l^*$; the results shown are consistent over multiple repeats. This repeatable abrupt changes in $l^*$ are likely not due to the coalescence of particles, as the latex volume fraction at this drying time is still low, at approximately 50 vol%. These abrupt changes may be caused by the transport or binding of particles to the film air–liquid interface, which would alter the fraction of photons entering the drying film and thus the transmitted light intensity. Thus, even without the more complex analyses of DWS or LSI experiments, a simple measurement of $l^*(t)$ may reveal the local microstructure of a drying film.

For the other three samples containing latex grades B, C, and D, $l^*(t)$ tended to decrease continuously and smoothly, approaching an equilibrium value $l^*(t) \approx 2$ µm as the film drying mass loss exited its quasi-linear domain. As these room-temperature experiments are below the glass transition temperature of the latex particles used for all inks, coalescence is not expected at any drying time, even when the latex volume fraction is extremely high; if coalescence does occur, $l^*(t)$ is expected to show a significant increase as the number of scattering interfaces abruptly decreases. For sample C, which started from a higher value of $l^*$, the initial decrease was even faster respect to B and D. We speculate that in the first part of the drying process, photons exploring the sample have more possibilities to travel various $l^*$ lengths before exiting the material.

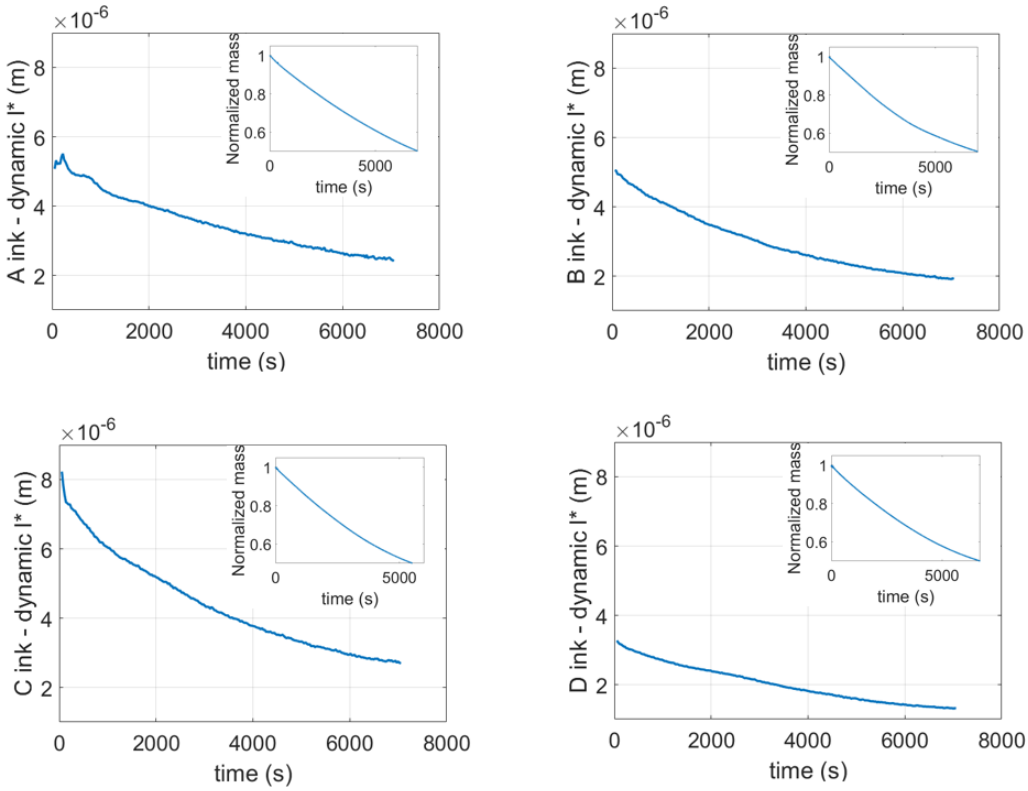


**Figure 4.** Dynamical evolution of $l^*$ for ink sample A, B, C, D for the first 7000 s after film creation. Insets: the corresponding relative mass loss.

We report in Appendix A, Figure A3, the relative $l^*$ *vs* mass loss for inks B, C, and D. The results confirm that $l^*$ initially decreases faster than the relative mass loss; this is consistent with previous experimental data [24], which also show that $l^*$ decreases faster than the linear volume fraction increases in agreement with the predicted hard-sphere Percus–Yevick structure factor, as seen in Figure 7 in [24]. While not measured, similar dynamic changes in $l^*(t)$ can be expected for inkjet-printed picoliter droplets, however, over a much more compressed timescale due to more rapid drying. In droplet experiments, there is a high probability that more of the collected photons exiting the liquid volume explore the scattering volume underneath the droplet. In this case, a fraction of the observable $l^*(t)$ arises also from the change in the substrate, caused by dispersion imbibement or fiber swelling in the very relevant case of paper substrates. To the best of our knowledge, these measurements of the changes in $l^*$ during the drying of a liquid film have not been studied before and are important to reliably prove that research involving multiple scattering experiments are valid for exploring and interpreting rapidly evolving microscopic-scale processes such as picoliter droplet evaporation.

## 4. Conclusions

We showed that $l^*$ is an essential parameter, often undervalued, to properly understand, interpret, and evaluate any multiply scattered light experiment, especially when the sample properties evolve over time. This parameter correlates to the volume of the sample that can be accessed with impinging photons. We showed that the measurement of scattered light intensity in a transmission geometry results in a facile and robust method to determine $l^*(t)$ compared with conventional measurement of the transport mean-free path length. Using the described setup, $l^*$ can be measured both for the case of static solid or liquid samples and measuring dynamic changes in $l^*$ for drying coatings films or inks droplets; ink droplet measurements are currently ongoing within our laboratory. In particular, we showed that in the case of drying ink films, $l^*$ tends to decrease during drying, initially faster than the mass loss and then approaching an equilibrium asymptotically only after the

rate of mass loss appears to alter from quasi-linearity. Importantly, the absolute value of $l^*$ found with this method validates the use DWS and LSI experiments on industrially relevant thin coatings, as all such pigment ink samples have an $l^*$ in the same order of magnitude, or even smaller, than the physical dimension of a drawn thin coating or a printed picoliter hemispherical droplet. This opens the door to further noninvasive measurements of drying coatings with multiple light scattering techniques that directly probe the in situ internal dynamics and structure of a drying coating. We did not observe a "bronzing effect", which has been an active area of research within the coating community; we speculate that a simultaneous combination of transmission $l^*$ determination and reflection spectroscopy would illuminate this topic further.

**Author Contributions:** Methodology, software. by R.A. Formal analysis, data curation, writing of the manuscript by both R.A. and T.E.K. Funding acquisition by T.E.K. All authors have read and agreed to the published version of the manuscript.

**Funding:** This research was funding through an OTP grant (15777) from the AES division of Nederlandse Organisatie voor Wetenschappelijk Onderzoek (NWO).

**Data Availability Statement:** Unprocessed and processed data are available through the corresponding author and will be made available through a public data repository when requested.

**Conflicts of Interest:** All authors declare no conflict of interest.

## Appendix A

**Table A1.** All inks were composed of 66 wt% water, 5 wt% pigment, 12 wt% latex, and 17 wt% glycerol. The latex composition was different for all four ink, resulting in small changes in the inks' physical properties: pH value, density, viscosity, and surface tension at 2 s after deposition.

| Sample Code | pH Value | Density (g/mL) | Viscosity (mPa·s) | ST@2s (mN/m) |
|---|---|---|---|---|
| A | 8.2 | 1.0697 | 4.1 | 54 |
| B | 8.4 | 1.0702 | 4.3 | 56 |
| C | 8.2 | 1.0697 | 4.6 | 63 |
| D | 8.3 | 1.0701 | 4.8 | 65 |

*Appendix A.1. Mass Measurements—Materials and Methods—Discussion*

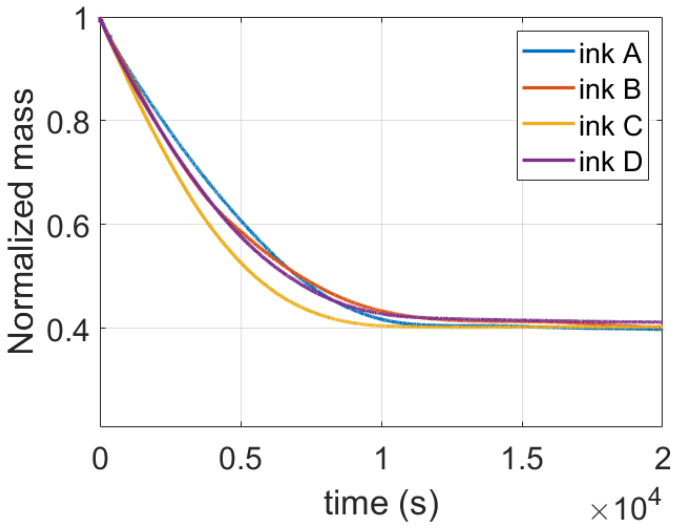


**Figure A1.** Normalized mass loss vs. time for the for inks corresponding to dynamic $l^*$ measurements.

Film mass was measured using an analytical balance. For each repetition, on a glass slide of dimensions 0.5 × 5 × 20 cm, we applied an ink film using a doctor blade of 0.150 mm thickness on the glass. Roughly 5 s after ink film deposition, the mass was measured for 20 × $10^3$ s at a rate of once per second. We performed the experiments for inks A, B, C, D. All the curves follow the same trend: a *quasi*-linear decrease for the first 4 × $10^3$ s, then reducing in drying rate, and finally asymptotically reaching a value around 40%, which is in close agreement with the starting values for the water content of the inks assuming some water content remains trapped in the ink film.

*Appendix A.2. Dynamic l* in the Case of Excessive Laser Power*

We present, in Figure A2, a dynamic measurement of $l^*$ for ink 3A, but operating at two different impinging laser powers: (a) 50 mW and (b) 350 mW at a 532 nm wavelength. We can observe that in case (a), the trend in $l^*$ is similar to the one reported for other inks in Figure 4: a fast decrease in the first period, followed by an asymptotic behavior towards the end of the drying process. This trend drastically changes while using a higher laser power, where we observe a rapid increase in $l^*$ after 1000 s. After 2000 s, we still recorded an increasing trend, but the measurement was halted for PMT over-saturation. This high laser power experiment shows that local heating of the film owing to excessive laser power leads to structural modification, degradation of the sample, and likely induces coalescence between the latex particles in the ink. We observe, at the laser spot location on the sample, a transparent region that grows in size with time. This degradation produces a more transparent material, where the $l^*$ parameter rapidly increases as more light, and therefore recorded intensity, travels through the ink film, reaching the detector.

*Appendix A.3. Dynamic l*(%) vs. Mass Loss (%)*

We present in Figure A3 the normalized mass loss with respect to the normalized mass loss that occurs during drying. We report for the three inks, B, C, and D, an initial decrease in $l^*$ faster than the mass loss. After this initial period, the two quantities decrease with a value close to a slope of 1, which would correspond to linear dependence.

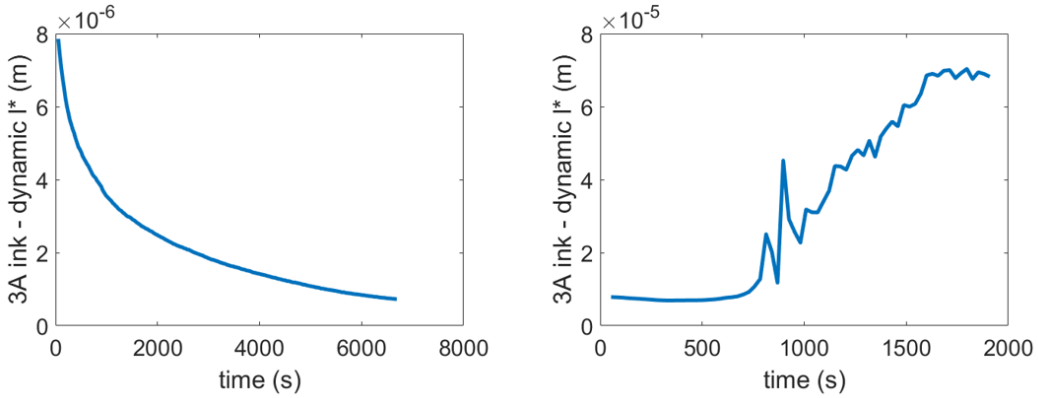


**Figure A2.** Two examples of calculated dynamic $l^*$ for the same ink in the cases of (**left**) 50 mW laser power and (**right**) 350 mW laser power. Note: the different scales in the *y* axis; thus, high laser power can lead to large changes in $l^*$, likely due to induced coalescence of latex particles within the drying film.

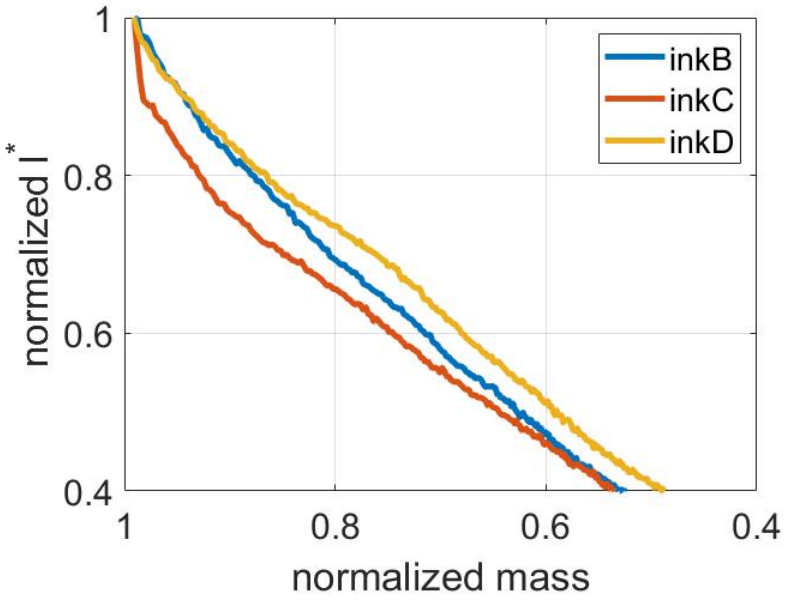


**Figure A3.** Normalized $l^*$ relative to the normalized mass loss for inks B, C, and D. Note the faster-than-linear drop in $l^*$ relative to mass loss, which would be a diagonal line in the plot.

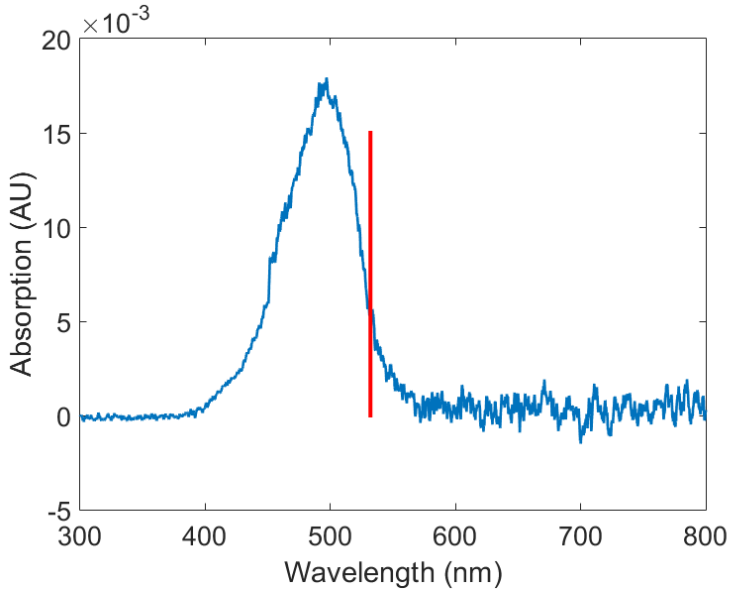


**Figure A4.** Absorption spectra of 0.15 mm thick film of ink A on white reference substrate card stock (BYK-Altana 2811, Vessel, Germany). The incident laser wavelength, 532 nm, is indicated by the vertical red line.

## References

1. Brenner, M.; Hilgenfeldt, S.; Lohse, D. Single-bubble sonoluminescence. *Rev. Mod. Phys.* **2002**, *74*, 425. [CrossRef]
2. Draijer, M.; Hondebrink, E.; Van Leeuwen, T.; Steenbergen, W. Review of laser speckle contrast techniques for visualizing tissue perfusion. *Lasers Med. Sci.* **2009**, *24*, 639–651. [CrossRef] [PubMed]
3. Lohse, D. Fundamental fluid dynamics challenges in inkjet printing. *Annu. Rev. Fluid Mech.* **2022**, *54*, 349–382. [CrossRef]
4. Van Der Kooij, H.; Fokkink, R.; Van Der Gucht, J.; Sprakel, J. Quantitative imaging of heterogeneous dynamics in drying and aging paints. *Sci. Rep.* **2016**, *6*, 34383. [CrossRef]
5. Lambourne, R.; Strivens, T. *Paint and Surface Coatings: Theory and Practice*; Elsevier: Amsterdam, The Netherlands, 1999.
6. Routh, A. Drying of thin colloidal films. *Rep. Prog. Phys.* **2013**, *76*, 046603. [CrossRef]
7. Zhang, Y.; Qian, Y.; Liu, Z.; Li, Z.; Zang, D. Surface wrinkling and cracking dynamics in the drying of colloidal droplets. *Eur. Phys. J. E* **2014**, *37*, 1–7. [CrossRef]

8. Zhang, C.; Fang, K. Surface modification of polyester fabrics for inkjet printing with atmospheric-pressure air/Ar plasma. *Surf. Coat. Technol.* **2009**, *203*, 2058–2063. [CrossRef]
9. Sharma, A.; Kakkar, S.; Chauhan, V.; Chakrabarti, S.; Varadhan, R. Efficacy of ASA sizing with agro-residue and recycled pulps using different fillers. *IPPTA Quart. J. Ind. Pulp. Paper Tech. Assoc.* **2012**, *24*, 93–98.
10. Daniel, R.; Berg, J. Spreading on and penetration into thin, permeable print media: Application to ink-jet printing. *Adv. Colloid Interface Sci.* **2006**, *123*, 439–469. [CrossRef]
11. Briers, J.; Richards, G.; He, X. Capillary blood flow monitoring using laser speckle contrast analysis (LASCA). *J. Biomed. Opt.* **1999**, *4*, 164–175. [CrossRef]
12. Briers, J.; Fercher, A. Retinal blood flow visualization by means of laser speckle. In *Optics in Biomedical Sciences: Proceedings of the International Conference, Graz, Austria, 7–11 September 1981*; Springer Publishing: Berlin/Heidelberg, Germany, 1982; pp. 158–161.
13. Cheng, H.; Luo, Q.; Zeng, S.; Chen, S.; Cen, J.; Gong, H. Modified laser speckle imaging method with improved spatial resolution. *J. Biomed. Opt.* **2003**, *8*, 559–564. [CrossRef] [PubMed]
14. Pieczywek, P.; Cybulska, J.; Zdunek, A.; Kurenda, A. Exponentially smoothed Fujii index for online imaging of biospeckle spatial activity. *Comput. Electron. Agric.* **2017**, *142*, 70–78. [CrossRef]
15. Kooij, H. Let There Be Light: Quantitative Imaging of Nanoscale Dynamics in Polymer Materials. Ph.D. Thesis, Wageningen University, Wageningen, The Netherlands, 2020.
16. Buijs, J.; Gucht, J.; Sprakel, J. Fourier Transform Laser Speckle Imaging for art conservation. *Bull. Am. Phys. Soc.* **2020**, *65*, 1.
17. Kooij, H.; Dussi, S.; Kerkhof, G.; Frijns, R.; Gucht, J.; Sprakel, J. Laser Speckle Strain Imaging reveals the origin of delayed fracture in a soft solid. *Sci. Adv.* **2018**, *4*, eaar1926. [CrossRef]
18. Cipelletti, L.; Ramos, L. Slow dynamics in glassy soft matter. *J. Phys. Condens. Matter* **2005**, *17*, R253. [CrossRef]
19. Scheffold, F.; Lenke, R.; Tweer, R.; Maret, G. Localization or classical diffusion of light? *Nature* **1999**, *398*, 206–207. [CrossRef]
20. Van Albada, M.; Lagendijk, A. Observation of weak localization of light in a random medium. *Phys. Rev. Lett.* **1985**, *55*, 2692. [CrossRef]
21. Akkermans, E.; Wolf, P.; Maynard, R.; Maret, G. Theoretical study of the coherent backscattering of light by disordered media. *J. Phys.* **1988**, *49*, 77–98. [CrossRef]
22. Pine, D.; Weitz, D.; Chaikin, P.; Herbolzheimer, E. Diffusing wave spectroscopy. *Phys. Rev. Lett.* **1988**, *60*, 1134. [CrossRef]
23. Maret, G. Diffusing-wave spectroscopy. *Curr. Opin. Colloid Interface Sci.* **1997**, *2*, 251–257. [CrossRef]
24. Weitz, D.; Zhu, J.; Durian, D.; Gang, H.; Pine, D. Diffusing-wave spectroscopy: The technique and some applications. *Phys. Scr.* **1993**, *1993*, 610. [CrossRef]
25. Scheffold, F.; Skipetrov, S.; Romer, S.; Schurtenberger, P. Diffusing-wave spectroscopy of nonergodic media. *Phys. Rev. E* **2001**, *63*, 061404. [CrossRef] [PubMed]
26. Duran-Ledezma, A.A.; Jacinto-Méndez, D.; Rojas-Ochoa, L.F. Time-resolved study of optical properties and microscopic dynamics during the drying of $TiO_2$ films by spectral diffusing wave spectroscopy. *Appl. Opt.* **2018**, *57*, 208. [CrossRef] [PubMed]
27. Lenke, R.; Maret, G. Multiple scattering of light: Coherent backscattering and transmission. In *Scattering in Polymeric and Colloidal Systems*; CRC Press: Boca Raton, FL, USA, 2000; pp. 1–73.
28. Jacucci, G.; Onelli, O.; De Luca, A.; Bertolotti, J.; Sapienza, R.; Vignolini, S. Coherent backscattering of light by an anisotropic biological network. *J. R. Soc. Interface Focus* **2019**, *9*, 20180050. [CrossRef]
29. Aegerter, C.; Maret, G. Coherent backscattering and Anderson localization of light. *Prog. Opt.* **2009**, *52*, 1–62.
30. Wang, L.; Jacques, S. Use of a laser beam with an oblique angle of incidence to measure the reduced scattering coefficient of a turbid medium. *Appl. Opt.* **1995**, *34*, 2362–2366. [CrossRef]
31. Lindbergh, T.; Larsson, M.; Fredriksson, I.; Strömberg, T. Reduced scattering coefficient determination by non-contact oblique angle illumination: Methodological considerations. *Opt. Interact. Tissue Cells XVIII* **2007**, *6435*, 119–130.
32. Yodh, A.; Kaplan, P.; Pine, D. Pulsed diffusing-wave spectroscopy: High resolution through nonlinear optical gating. *Phys. Rev. B* **1990**, *42*, 4744. [CrossRef]
33. Mikhailovskaya, A.; Fade, J.; Crassous, J. Speckle decorrelation with wavelength shift as a simple way to image transport mean free path. *Eur. Phys. J. Appl. Phys.* **2019**, *85*, 30701. [CrossRef]
34. Rojas, L.F.; Bina, M.; Cerchiari, G.; Escobedo-Sánchez, M.A.; Ferri, F.; Scheffold, F. Photon path length distribution in random media from spectral speckle intensity correlations. *Eur. Phys. J. Spec. Top.* **2011**, *199*, 167. [CrossRef]
35. Aubry, G.J.; Fuchs, N.; Skipetrov, S.; Scheffold, F. Transport properties of optically thin solid dielectrics from frequency correlations of randomly scattered light. *Opt. Lett.* **2022**, *47*, 1439. [CrossRef] [PubMed]
36. Zhang, C.; Reufer, M.; Gaudino, D.; Scheffold, F. Improved diffusing wave spectroscopy based on the automatized determination of the optical transport and absorption mean free path. *Korea-Aust. Rheol. J.* **2017**, *29*, 241–247. [CrossRef]
37. Weitz, D.; Pine, D.; Pusey, P.; Tough, R. Nondiffusive Brownian motion studied by diffusing-wave spectroscopy. *Phys. Rev. Lett.* **1989**, *63*, 1747. [CrossRef] [PubMed]
38. Viasnoff, V.; Lequeux, F.; Pine, D. Multispeckle diffusing-wave spectroscopy: A tool to study slow relaxation and time-dependent dynamics. *Rev. Sci. Instrum.* **2002**, *73*, 2336–2344. [CrossRef]
39. Pine, D.; Weitz, D.; Zhu, J.; Herbolzheimer, E. Diffusing-wave spectroscopy: Dynamic light scattering in the multiple scattering limit. *J. Phys.* **1990**, *51*, 2101–2127. [CrossRef]
40. MacKintosh, F.; Zhu, J.; Pine, D.; Weitz, D. Polarization memory of multiply scattered light. *Phys. Rev. B* **1989**, *40*, 9342. [CrossRef]

41. Bonnet, C.; Corredig, M.; Alexander, M. Stabilization of caseinate-covered oil droplets during acidification with high methoxyl pectin. *J. Agric. Food Chem.* **2005**, *53*, 8600–8606. [CrossRef]
42. Alexander, M.; Rojas-Ochoa, L.; Leser, M.; Schurtenberger, P. Structure, dynamics, and optical properties of concentrated milk suspensions: An analogy to hard-sphere liquids. *J. Colloid Interface Sci.* **2002**, *253*, 35–46. [CrossRef]
43. Durian, D.; Weitz, D.; Pine, D. Multiple light-scattering probes of foam structure and dynamics. *Science* **1991**, *252*, 686–688. [CrossRef]
44. Yang, L. Characterization of inks and ink application for ink-jet printing: Model and simulation. *J. Opt. Soc. Am. A* **2003**, *20*, 1149–1154. [CrossRef]
45. Gross, P.; Störzer, M.; Fiebig, S.; Clausen, M.; Maret, G.; Aegerter, C. A precise method to determine the angular distribution of backscattered light to high angles. *Rev. Sci. Instrum.* **2007**, *78*, 033105. [CrossRef] [PubMed]

**Disclaimer/Publisher's Note:** The statements, opinions and data contained in all publications are solely those of the individual author(s) and contributor(s) and not of MDPI and/or the editor(s). MDPI and/or the editor(s) disclaim responsibility for any injury to people or property resulting from any ideas, methods, instructions or products referred to in the content.